scientific reports

Check for updates

OPEN

Effects of gravel columns on static and dynamic properties of sand: a laboratory investigation

Gui Yang✉, Jiaxuan Gao, Yiheng Zhang & Qian Feng

Vibrated stone columns (composed of gravel in this study) are widely used for ground improvement. However, the composite behavior of sand–gravel composite columns (SGCC) under combined static and dynamic loading is not yet fully understood. This study systematically investigates the static and dynamic properties of SGCC through consolidated drained, consolidated undrained, and cyclic triaxial tests. The results show that gravel columns enhance the strength and deformation characteristics of SGCC through suppression of shear dilatancy. Under drained conditions, the peak strength ratio between SGCC and sand decreases with increasing confining pressure, whereas under undrained conditions, the ratio exhibits a positive correlation with confinement. The failure stress ratio of SGCC is 1.1 times that predicted by the conventional composite modulus method (CMM). The dynamic shear modulus and damping ratio of SGCC follow trends similar to those of sand and gravel, following a hyperbolic distribution. Compared with sand, SGCC exhibits an increased dynamic shear modulus and a reduced damping ratio. The dynamic modulus coefficient of SGCC is 1.2 times, and the damping ratio parameter is 1.5 times, the values estimated by CMM. Furthermore, the dynamic strength of SGCC is 1.1 times that of sand. These findings reveal the limitations of conventional CMM predictions and provide refined parameters, improving seismic safety design for stone-column foundations.

Keywords Sand-gravel composite column, Failure stress ratio, Dynamic shear modulus, Damping ratio, Dynamic strength

Soft soil foundations present major geotechnical challenges including low strength, high compressibility, and liquefaction potential, which can cause excessive settlement and structural failure. Vibrated stone columns (composed of gravel in this study) serve as a widely used ground improvement technique to address these issues by enhancing stability, reducing settlement, and mitigating seismic risk[1–4]. This study provides a mechanistic understanding of the composite behavior of gravel-column reinforced soils, offering critical insights for optimizing foundation design under both static and dynamic loading conditions.

The strength and deformation characteristics of foundations are therefore critical concerns in geotechnical design. Research on soft soil foundations reinforced with stone columns can generally be divided into two categories: one approach considers the stone columns as structural elements, while the other treats the stone columns and surrounding soil as a composite foundation system.

Extensive studies have been conducted through laboratory and field model tests. Ghazavi and Nazari[5] investigated the failure modes of single and grouped stone columns with varying diameters in low-strength soil using large-scale laboratory testing. Bulging failure typically occurs at a depth of 1D to 2D from the stone column head. The failure mode of stone columns was found to be a combination of bulging and lateral deformation. Murugesan and Rajagopal[6] demonstrated that lateral extrusion can lead to complete failure of stone columns, and recommended increasing their lateral deformation resistance.

The effectiveness of stone column treatment for soft foundations depends on many factors, including the area replacement ratio[7,8], column diameter[5], and column length[9,10]. Among these, the area replacement ratio is considered a key parameter in the design of composite foundations[11–13], as increasing it improves the bearing capacity and reduces the settlement of the composite foundation. Ambily and Gandhi[14], as well as Singh and Sahu[15], conducted tests on single and grouped stone columns, revealing that columns spaced beyond three times their diameter exhibit negligible group effect.

Stone columns primarily serve the functions of densification, drainage and stress reduction in mitigating the effects of liquefaction[16,17]. Among these, densification is the most dominant mechanism at lower soil densities, while drainage and stress reduction become more significant at higher densities. Relevant studies

State Key Laboratory of Precision Blasting, College of Civil and Transportation Engineering, Hohai University, Nanjing 210024, China. ✉email: ygheitu@163.com

have been conducted on the influence of stone columns on the dissipation of excess pore pressure and the acceleration response of composite foundations during seismic excitation[18,19]. Seismic loading causes stress redistribution due to changes in the initial stress state and stiffness of the foundation. When the stone columns and surrounding soil act in coordination, the seismic shear stress is distributed based on relative stiffness, with a greater proportion concentrated in the stone columns, thereby significantly reducing the shear stress transmitted to the surrounding soil. To account for stress discrepancies observed in 1 g shaking table model tests, centrifuge model tests have been conducted, and similar conclusions were reached[20–22]. Based on these centrifuge tests, Li et al.[23] employed a two-dimensional liquefaction model to analyze the plane strain behavior of stone columns, treating them as stone walls with equivalent stiffness. The results demonstrated that the reinforcement effect of stone columns can be accurately simulated using an appropriate constitutive model.

In actual engineering, stone columns are generally used over large areas for soft ground treatment, for example, when constructing rockfill dams on soft clay foundations[24]. It is very difficult to consider the role of each individual stone column during structural deformation and stability analysis. Therefore, stone columns and soil are usually analyzed as a composite material system[25]. Some studies involving geotextile-encased stone columns and soil composites[26–30] were conducted based on laboratory tests. The results of Najjar et al.[31] demonstrated that sand columns can effectively improve the shear strength of soft clay. An increase in the column length and area replacement ratio led to higher shear strength and lower water pressure. However, increasing the area replacement ratio did not significantly enhance the shear stiffness of the composite material, particularly at smaller shear strains[11]. The dynamic response of geotextile-encased grouped stone columns differs significantly from their static behavior[32]. High loading frequencies may reduce both bearing capacity and load transfer efficiency. Excess pore water pressure exhibits frequency dependency, with higher frequencies generating greater excess pore pressure ratios. Notably, encased stone columns demonstrate superior drainage performance compared to conventional stone columns[33].

Despite the extensive research on stone columns, most previous studies have focused on their group effect, encasement techniques, or numerical simulations under static conditions. However, the mechanical behavior of sand–gravel composite columns (SGCC) under cyclic loading has not been systematically investigated. The strength, deformation, and pore pressure response of SGCC under dynamic conditions remain poorly understood, which limits the accurate assessment of their performance in seismic-prone regions.

This study aims to bridge this gap through a comprehensive laboratory investigation involving consolidated drained (CD), consolidated undrained (CU), and cyclic triaxial tests on sand, gravel, and SGCC specimens. The experimental program evaluated the strength, volumetric change, and pore pressure evolution under both drained and undrained conditions, alongside the influence of sand and gravel on the composite foundation's static behavior. Furthermore, dynamic responses—including dynamic shear modulus, damping ratio, and dynamic strength—were analyzed to provide new insights for improving the seismic design of stone column-reinforced foundations.

Although numerous studies have investigated stone columns or surrounding soils, two major limitations persist. Most existing research focuses exclusively on either static or dynamic behavior, with limited integrated analysis of SGCC under combined loading conditions. Furthermore, the predictive accuracy of the Composite Modulus Method (CMM) for key composite parameters lacks experimental verification. To address these gaps, this study employs an integrated experimental approach to systematically examine the strength, deformation, and pore pressure behavior of SGCC. The results provide quantitative validation of the CMM and propose empirical correction factors for improved engineering predictions.

Laboratory testing

Test material and equipment

The materials used in the tests were Fujian standard sand from China and 2–5 mm gravel derived from sandstone parent rock. The particle size distribution curves of the sand and gravel are presented in Fig. 1.

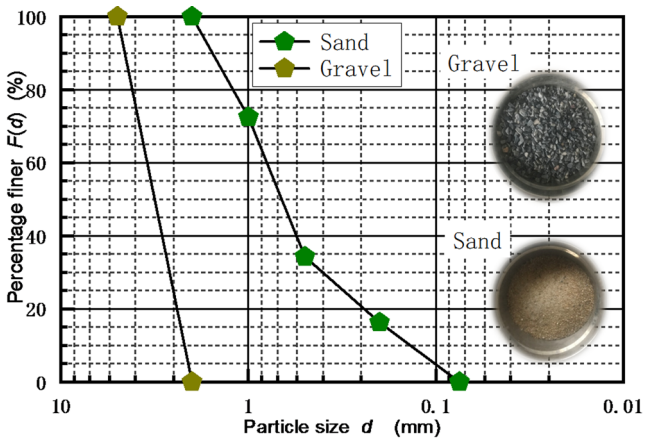

Fig. 1. Particle size distributions of the sand and the gravel.

The coefficient of uniformity (C_u) and coefficient of curvature (C_c) for the sand were 5.7 and 1.65, respectively. The maximum and minimum dry densities of sand were 1.83 g/cm^3 and 1.55 g/cm^3, respectively, while those of the gravel were 1.71 g/cm^3 and 1.43 g/cm^3. The relative density of reinforced foundation is generally required to exceed 0.6. In this study, a relative density of 0.8 was adopted for both sand and gravel, consistent with typical design specifications for stone columns in load-bearing applications. This density ensures adequate compaction to not only improve bearing capacity but also enhance liquefaction resistance and reduce seismic settlements. The corresponding dry densities of the sand and gravel at this relative density were 1.76 g/cm^3 and 1.64 g/cm^3, respectively.

The static and dynamic tests were performed using a conventional strain-controlled triaxial system and a GDS cyclic triaxial apparatus, respectively, as shown in Fig. 2. The GDS system features an axial load capacity of 10 kN, a frequency range of 0.01–5 Hz, and a maximum confining pressure of 1.0 MPa.

Test procedure

The sand and gravel samples were prepared as conventional cylindrical specimens with diameters of 39.1 mm and 100 mm, respectively. These specimens were constructed using the layered compaction method in five layers, with the mass of material for each layer carefully controlled to achieve the target relative density of 0.8. The height of each layer was monitored during compaction to ensure uniform density throughout the specimen, following standard laboratory procedures for triaxial sample preparation.

The SGCC samples, 100 mm in diameter, were prepared using a method different from that for the pure sand and gravel samples. The equipment used for sample preparation included a steel pipe, internal hammer, external hammer, and ring gasket. The outer diameter, wall thickness, and length of the steel pipe were 35 mm, 1 mm, and 300 mm, respectively. The outer diameter of the internal hammer was 30 mm, while the outer diameter and inner diameter of the external hammer were 60 mm and 37 mm, respectively. The ring gasket had an outer diameter of 96 mm and an inner diameter of 37 mm. The samples were prepared in 5 layers using a layered filling method. The steel pipe was gradually lifted as the filling height increased, and its embedded depth in the soil was twice the thickness of each layer, except for the first layer.

It is worth noting that this sample preparation method was specifically designed to simulate the key feature of a compacted stone column surrounded by soil. Although it does not replicate the full-scale field installation process, it effectively creates a well-defined composite interface and achieves a high, uniform relative density, which is representative of well-constructed stone columns. To ensure reproducibility and uniformity, the process was highly standardized: each layer was compacted to a fixed height with controlled energy. Figure 3(a) illustrates the position of the steel pipe and the preparation equipment during the filling of the third layer. The completed sample is shown in Fig. 3(b). The volume ratio of sand to gravel in SGCC was 7.16. This ratio corresponds to a practical area replacement ratio of 12%, which falls within the common design range (10%–20%) recommended in ground improvement.

The experimental program included both CD and CU triaxial shear tests. These tests were designed to evaluate long-term drained and short-term undrained strength characteristics respectively. The specimen preparation and loading process were conducted in accordance with MWR (GB/T 50123 – 2019)[34]. Prior to shearing, the specimens were saturated by allowing water to flow through the base of the triaxial cell. When the Skempton's B-value was less than 95%, back pressure saturation was employed. The specimens were then isotropically consolidated under effective confining pressures of 100 kPa, 200 kPa, and 300 kPa, which were selected to represent in-situ stress conditions from shallow to moderate depths.

The monotonic shearing was performed at a constant displacement rate of 0.04 mm/min. All tests were terminated at a maximum axial strain of 16% in accordance with MWR (GB/T 50123 – 2019)[34] and due to

Fig. 2. Static and cyclic triaxial test equipment.

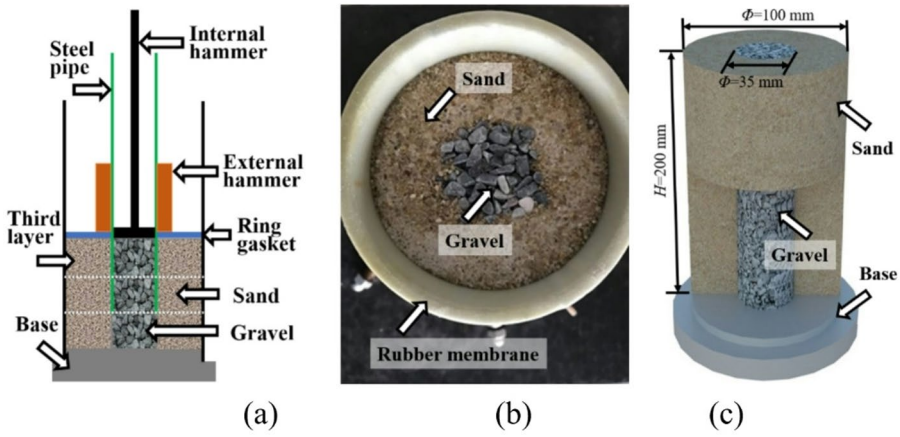

Fig. 3. Preparation tools and sample of SGCC. (**a**) Compaction tools, (**b**) Prepared sample, (**c**) Schematic diagram.

equipment limitations. A load sensor and a pore-pressure sensor were used to measure the deviator load, drainage volume, and pore pressure, respectively. Cyclic triaxial tests were conducted under stress-controlled and undrained conditions. A sinusoidal load was applied at a frequency of 1.0 Hz. During the tests, the axial force, pore water pressure, and axial displacement of the specimens were continuously recorded.

The area replacement ratio (A_{rr}) is an important parameter for stone column reinforced soft ground. It is conventionally defined as the ratio of the area of the stone column to the tributary area, as shown follow[31,35]:

$$A_{rr} = A_g / A_s \tag{1}$$

where A_g is the cross-sectional area of the stone column, and A_s is the cross-sectional area of the specimen. In the test, the area replacement ratio was 0.12.

Static results analysis

The stress parameters used in this study are the mean effective stress (p') and deviator stress (q). In triaxial tests, these parameters are defined as follows:

$$p' = \left(\sigma_1' + 2\sigma_3'\right)/3 \tag{2}$$

$$q = \sigma_1' - \sigma_3' \tag{3}$$

where σ_3' is the effective confining pressure, and σ_1' is the effective axial stress.

Stress-strain behavior

Figure 4. presents the stress-strain responses of sand, gravel, and SGCC under CD tests. The stress-strain curve of SGCC exhibits a distinct reverse bending phenomenon at the initial stage of shearing, which is different from that of sand and gravel. The mechanical behavior of SGCC is more similar to that of sand than gravel. Both SGCC and sand exhibit significant strain softening behavior, which becomes more pronounced with increasing confining pressure. In contrast, the strain softening behavior in the gravel specimen is not obvious.

The peak strain – defined as the axial strain corresponding to the peak stress – for sand decreases with increasing confining pressure, with values of 4.2%, 4.1%, and 3.9% under confining pressures of 100 kPa, 200 kPa, and 300 kPa, respectively. In contrast, SGCC shows the opposite trend: the peak strain increases with confining pressure, with corresponding values of 3.2%, 4.9%, and 5.4%, respectively.

SGCC exhibited the highest peak strength across all confining pressures (e.g., 784.6, 765.0, and 660.3 kPa for SGCC, gravel, and sand, respectively, at σ_3 = 200 kPa). This enhancement resulted from the composite action of the gravel column, which improved stress transfer and provided additional confinement to the sand matrix. Although prepared at identical relative density, the gravel specimen had a lower dry density than sand, yet still achieved higher strength due to its superior frictional resistance and particle interlocking.

This indicates that the addition of gravel to sand can effectively enhance its strength. The ratios of peak strength of SGCC to that of sand under different confining pressures (σ_3 = 100 kPa, 200 kPa, and 300 kPa) are 1.35, 1.19, and 1.12, respectively. As the confining pressure increases, the reinforcement effect of gravel in SGCC diminishes. However, the residual strength of SGCC is similar to that of sand. For example, at an axial strain of 16% and a confining pressure of 300 kPa, the strengths of sand and SGCC are 855.3 kPa and 852.4 kPa, respectively. Therefore, in practical engineering applications, the reinforcement efficiency of gravel columns gradually decreases with increasing depth.

The decrease in the strength improvement ratio (from 1.35 to 1.12) with increasing confining pressure is attributed to the diminishing stiffness contrast between the gravel column and the surrounding soil. At low

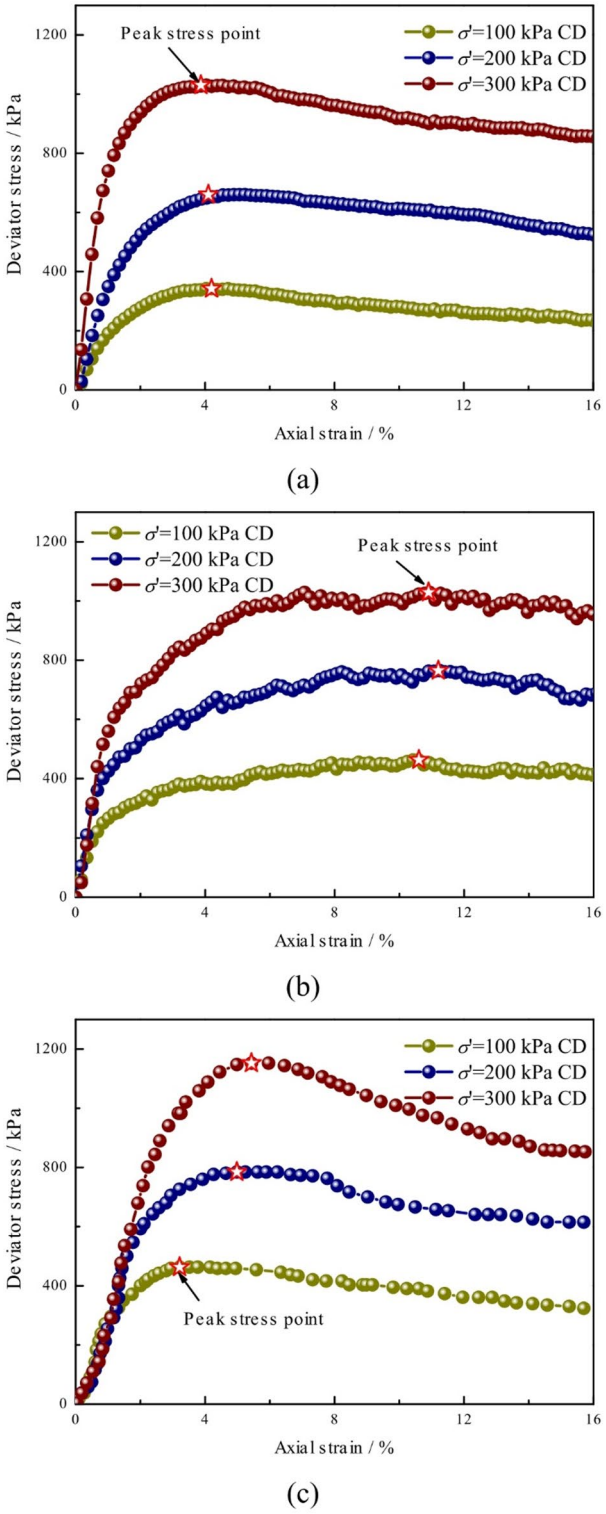

Fig. 4. Deviator stress-axial strain curves for all samples under CD conditions. (**a**) sand, (**b**) gravel, (**c**) SGCC.

confining pressures (i.e., shallow depths), the soft soil permits significant stress concentration on the stiff column, resulting in high reinforcement efficiency. In contrast, at high confining pressures (i.e., greater depths), the surrounding soil becomes stiffer, reducing the stiffness contrast. Consequently, the applied load is more evenly distributed, thereby diminishing the column's relative contribution. This finding explains why gravel columns are most effective for shallow foundation improvement, whereas their efficiency in deep applications requires careful evaluation.

Figure 5 presents the stress-strain curves of sand, gravel and SGCC under CU tests. The stress-strain behavior under CU conditions is similar to that observed in the CD tests. The peak strength of SGCC increases from 463.2 kPa to 1152.5 kPa, representing a 3.10-fold increase at a confining pressure of 100 kPa. However, as the confining pressure increases, the rate of strength increase gradually decreases. For example, when the confining pressure increases from 200 kPa to 300 kPa, the strength increases factor decreases from 2.24 to 1.87. Sand and gravel exhibit similar trends to SGCC, among which gravel has the lowest strength growth rate, followed by SGCC, while sand shows the highest rate of increase.

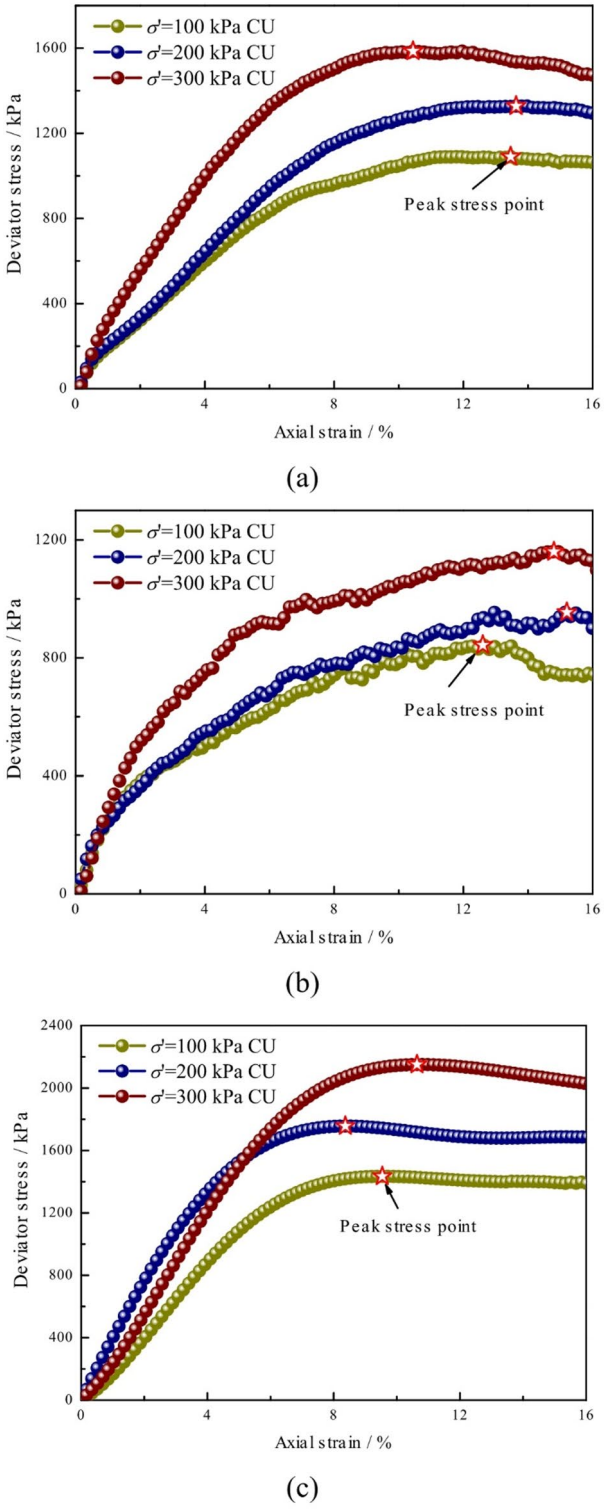

Fig. 5. Deviator stress-axial strain curves for all samples under CU conditions. (**a**) sand, (**b**) gravel, (**c**) SGCC.

The peak strength of SGCC is the highest, followed by sand, while gravel exhibits the lowest peak strength. Compared with the CD test, the peak stress ratio increases under higher confining pressures. The ratios of peak strength of SGCC to that of sand under different confining pressures (σ_3 = 100 kPa, 200 kPa, and 300 kPa) are 1.32, 1.32, and 1.36, respectively. The strength increases results primarily from the high relative density of the specimen and its dilatant behavior during shearing. This dilatancy induces negative pore water pressure, thereby increasing the effective stress.

Volume strain behavior

Figure 6 presents the volume strain–axial strain curves of sand, gravel, and SGCC under CD tests. Positive volume strain indicates compression, while negative volume strain reflects dilation. With increasing shear strain, the specimens initially contract and subsequently dilate. The axial strain corresponding to the onset of dilation increases with the confining pressure. For example, the axial strains at the dilation point for SGCC are 1.1%, 2.0%, and 2.1% under confining pressures of 100 kPa, 200 kPa, and 300 kPa, respectively.

At low strain levels, the volume strain difference between sand and SGCC is minimal, but the difference gradually increases with increasing strain. Before the axial strain reaches 8%, the two curves approximately coincide under a confining pressure of 100 kPa. However, when the axial strain reaches 8%, an obvious turning point in volume strain appears for SGCC, and the rate of volume strain increase decreases significantly. This behavior may be attributed to the dilatancy of gravel being much less pronounced than that of sand.

Similarly, under a confining pressure of 200 kPa, a turning point is also observed, but the axial strain at the turning point is higher than that under 100 kPa. However, at a confining pressure of 300 kPa, SGCC does not exhibit a distinct turning point; instead, it enters a stable state earlier than sand. This crucial observation can be attributed to the inhibiting effect of confinement on particle rearrangement. At lower confining pressures, the relatively weak lateral restraint permits progressive dislocation and lateral bending of the stiff gravel column during shearing, which results in a sudden change in the dilation rate (manifesting as a clear turning point, see Fig. 7(a)). In contrast, at a confining pressure of 300 kPa, the substantially enhanced lateral constraint effectively "locks" the gravel column and suppresses its dislocation. Consequently, the entire composite undergoes more homogeneous and constrained dilatancy, leading to a smooth transition without a sharp turning point. This mechanism is consistent with the observed bulging-like failure mode under high confinement, which does not exhibit the sharp shear bands caused by dislocation (Fig. 7(b)).

Pore pressure analysis

Figure 8 presents the pore pressure-axial strain curves of sand, gravel and SGCC under CU tests. It has been shown that back pressure affects the results of CU tests; therefore, a constant back pressure of 430 kPa was applied to saturate all samples. With increasing confining pressure, the pore pressure responses of SGCC and sand vary significantly. Due to the large voids within the gravel, pore pressure is difficult to accumulate.

As axial stain increases, the pore pressure first rises and then declines. The maximum pore pressure increases with increasing confining pressure and typically occurs at an axial strain range of 0.5% to 1.0%. After reaching a certain axial strain, the pore pressure gradually stabilizes, a behavior that is particularly pronounced in SGCC.

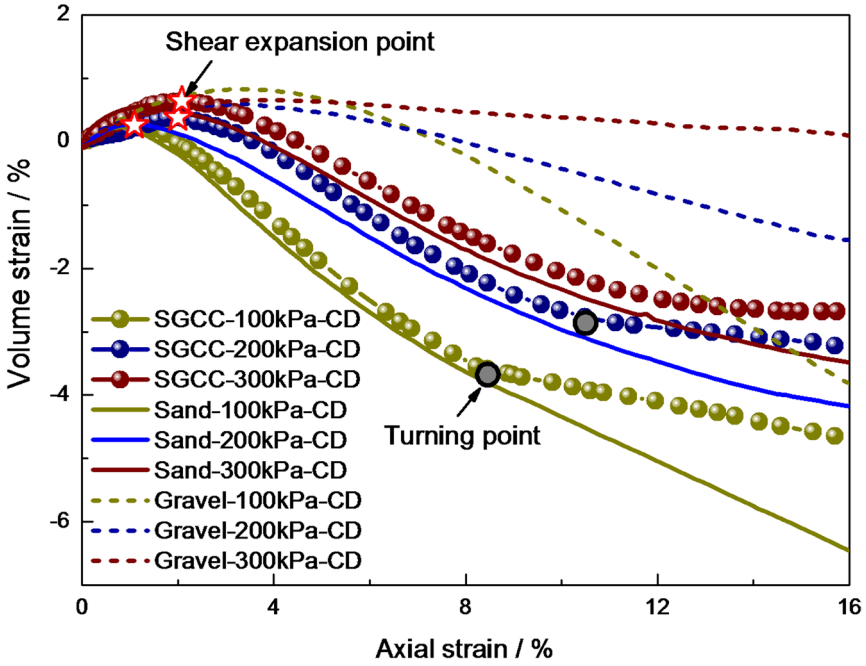

Fig. 6. Volumetric strain-axial strain curves for all samples under CD conditions.

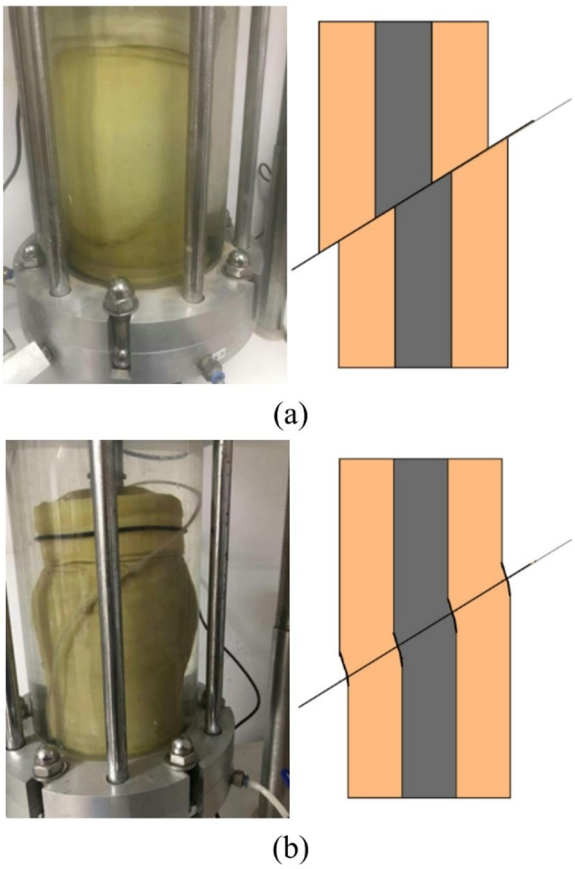

Fig. 7. Failure surface of the SGCC sample. (**a**) confining pressure 100 kPa, (**b**) confining pressure 300 kPa.

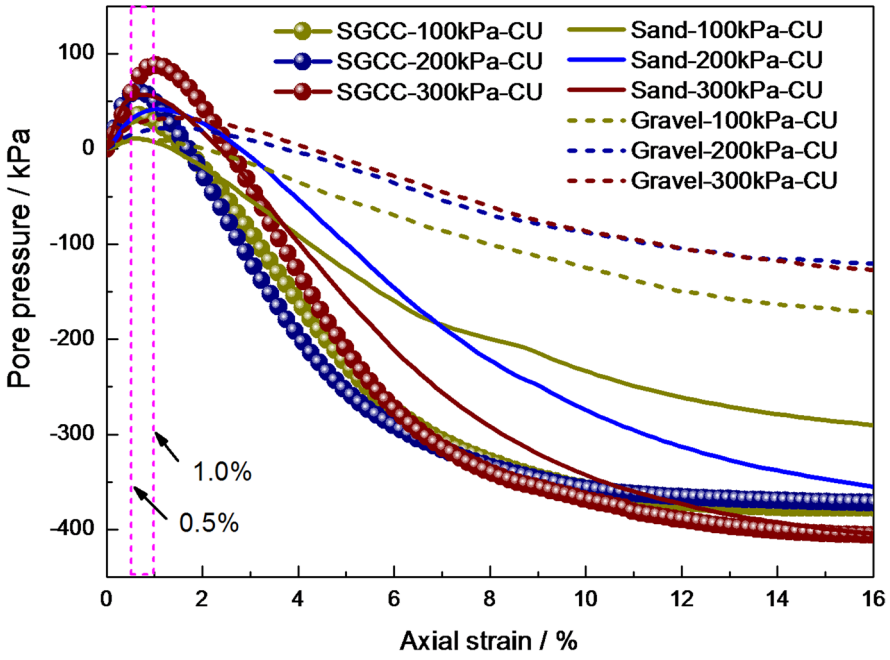

Fig. 8. Pore pressure-axial strain curves for all samples under CU conditions.

This is primarily because the gravel columns in SGCC promote earlier dilatancy, allowing the specimen to reach a stable state earlier than the sand specimen.

The difference in pore pressure between SGCC and sand is more evident under low confining pressure, but this difference gradually decreases as confining pressure increases, eventually tending toward consistency. This result may be attributed to gravel column dislocation during the shearing process of SGCC under low confining pressure, where fine particles infiltrate the voids between gravel particles, leading to a reduction in permeability.

P-q change behavior

Figure 9 illustrates the effective stress paths of sand, gravel, and SGCC under the CD and CU tests. It can be seen that the effective stress paths of the specimens diverge prior to reaching the peak state, due to the influence of different confining pressures. At the peak state, the stress paths under different confining pressures converge and exhibit a linear upward trend. Beyond the peak state, the effective stress paths diverge again and gradually decline until a critical state is reached.

The peak stress points obtained from the CD and CU tests for sand, gravel, and SGCC can be fitted using a straight line. The corresponding expression is given as follows:

$$q_f = M_f p_f \tag{4}$$

where M_f is the failure stress ratio; q_f is the peak deviator stress; p_f is the mean effective stress corresponding to q_f.

The failure stress ratio of gravel is the highest (M_f=1.60), followed by SGCC (M_f=1.57), and sand exhibits the lowest value (M_f=1.40). Referring to the composite modulus method (CMM), the equivalent failure stress ratio for the improved area can be estimated based on the properties of individual gravel columns and soft soil, as well as the area replacement ratio[36,37], as follows:

$$M_{feq} = M_{fc} A_{rr} + M_{fs} (1 - A_{rr}) \tag{5}$$

where M_{feq} is the equivalent failure stress ratio of SGCC; M_{fc} and M_{fs} are the failure stress ratio of gravel and sand, respectively.

The failure stress ratio of SGCC obtained from the test is approximately 1.1 times that predicted by CMM (M_{feq} =1.42).

Dynamic results analysis

Dynamic shear modulus and damping ratio are two key parameters that characterize the dynamic behavior of soils and serve as important indicators for evaluating seismic response and seismic safety. The dynamic shear modulus (G_d), dynamic shear stress (τ_d), and dynamic shear strain (γ_d) are calculated using the following equations:

$$G_d = \tau_d / \gamma_d \tag{6}$$

$$\tau_d = q_d / 2 \tag{7}$$

$$\gamma_d = (1 + \mu)\, \varepsilon_d \tag{8}$$

where q_d is the dynamic stress; ε_d is the dynamic axial strain; μ is Poisson's ratio, which is taken as 0.5 for undrained conditions[38].

Dynamic shear modulus analysis

Figure 10 shows the relationship between dynamic shear modulus and dynamic shear strain for sand, gravel, and SGCC under different confining pressures. The variation pattern of dynamic shear modulus with dynamic shear strain is similar for all three materials. The dynamic shear modulus decreases nonlinearly with increasing dynamic shear strain, and increases with increasing confining pressure. Among the three materials, gravel exhibits the highest dynamic shear modulus, followed by SGCC, while sand shows the lowest. The higher dynamic shear modulus of SGCC compared to sand results from micromechanical interactions between the materials. Rigid gravel particles embedded in the sand form a reinforced force-chain network. Interlocking between angular sand particles and coarse gravel surfaces increases resistance to shear deformation, enhancing overall stiffness. Additionally, the inherently higher modulus of gravel further contributes to the composite's rigidity.

Due to limitations of the testing equipment, the maximum dynamic shear modulus (G_{max}) could not be directly measured. Instead, G_{max} was estimated through curve fitting[39,40].

Figure 11 plots the relationship between maximum dynamic shear modulus and mean effective stress for sand, gravel, and SGCC. Numerous empirical equations have been developed to describe the relationship between confining pressure and void ratio with the maximum dynamic shear modulus[41,42]. This relationship can be expressed as follows[42]:

$$G_{\max} = k p_a \left(\frac{\sigma_m}{p_a} \right)^n \tag{9}$$

where σ_m is the initial mean effective stress, σ_m=(2 + k_c)σ_3'/3; k and n are empirical model parameters; k_c is the consolidation stress ratio (k_c = 1.0); and p_a is the atmospheric pressure (p_a=101 kPa).

Using curve fitting based on Eq. (9), the model parameters were obtained and are summarized in Table 1. It can be seen that the dynamic shear modulus parameters of SGCC lie between those of sand and gravel. The

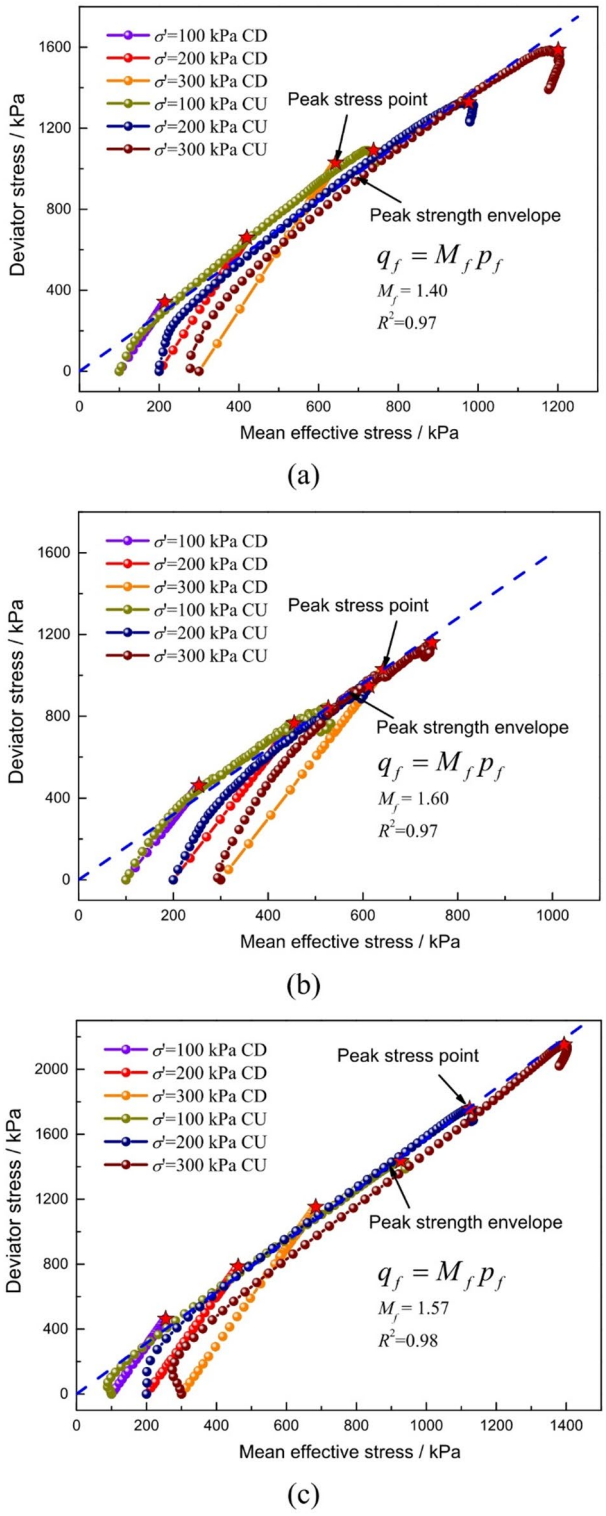

Fig. 9. Effective stress paths for all samples in CD and CU tests. (**a**) Sand, (**b**) Gravel, (**c**) SGCC.

parameters *n* and *k* of SGCC are 1.0 and 1.2 times, respectively, the values according to CMM, and are calculated as follows:

$$n_{eq} = n_g A_{rr} + n_s (1 - A_{rr}) \tag{10}$$

$$k_{eq} = k_g A_{rr} + k_s (1 - A_{rr}) \tag{11}$$

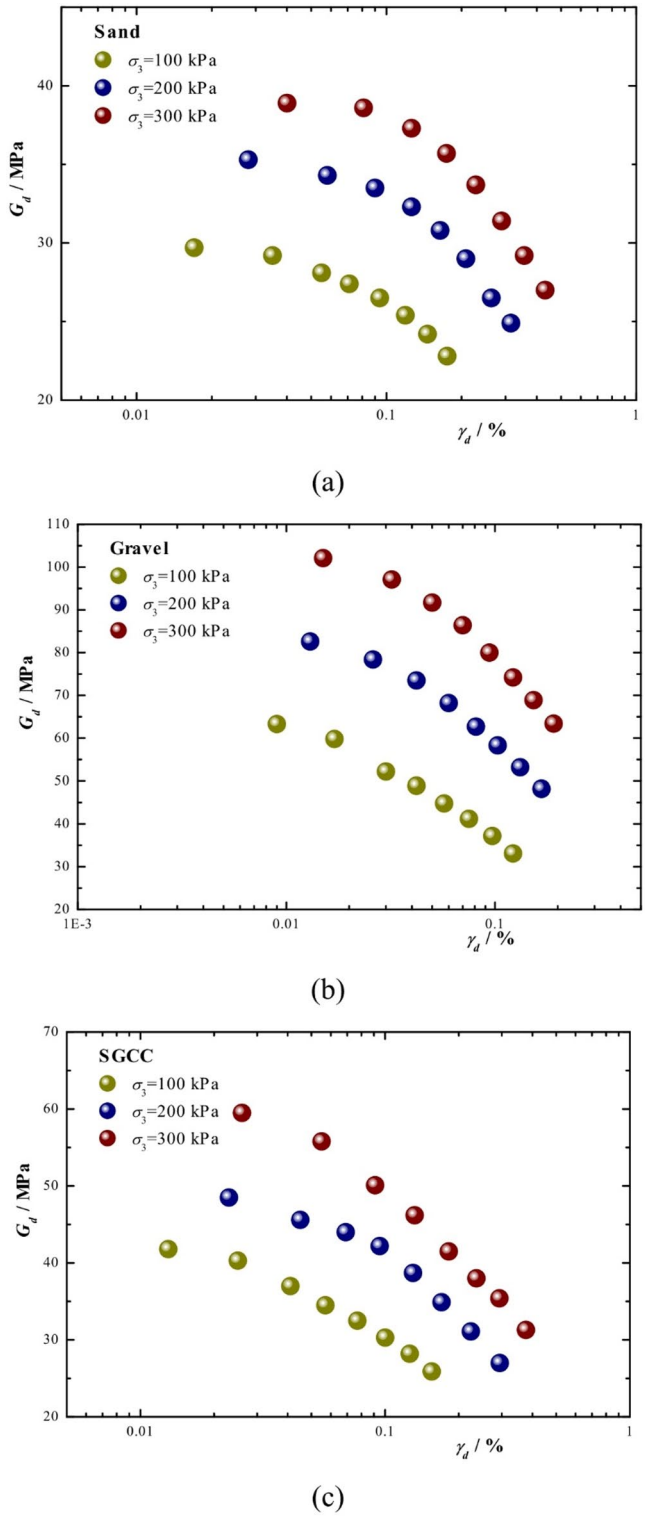

Fig. 10. G_d versus γ_d relationships for all samples under different confining pressures. (**a**) Sand, (**b**) Gravel, (**c**) SGCC.

where n_g and n_s are the modulus parameters of gravel and sand, respectively; k_g and k_s are the modulus parameters of gravel and sand, respectively.

Figure 12 shows the normalized dynamic shear modulus (G_d/G_{max}) versus normalized dynamic shear strain (γ_d/γ_r) for sand, gravel, and SGCC. The differences among the three materials are relatively small and fall within a narrow range. The data were fitted using the following expression[43]:

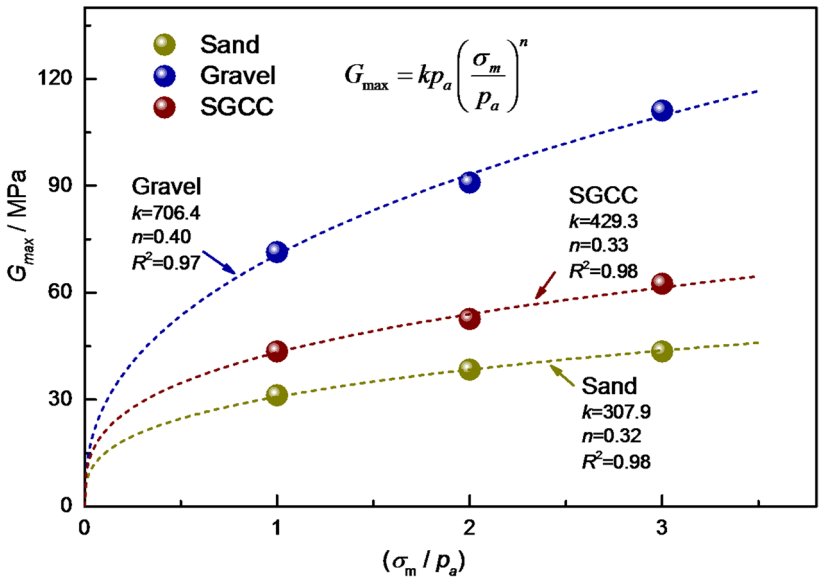

Fig. 11. G_{max} versus σ_m/p_a for all samples under different confining pressures.

Parameters	Sand	Gravel	SGCC	CMM
k	307.9	706.4	429.3	356.7
n	0.32	0.40	0.33	0.33

Table 1. Model parameters of maximum shear modulus.

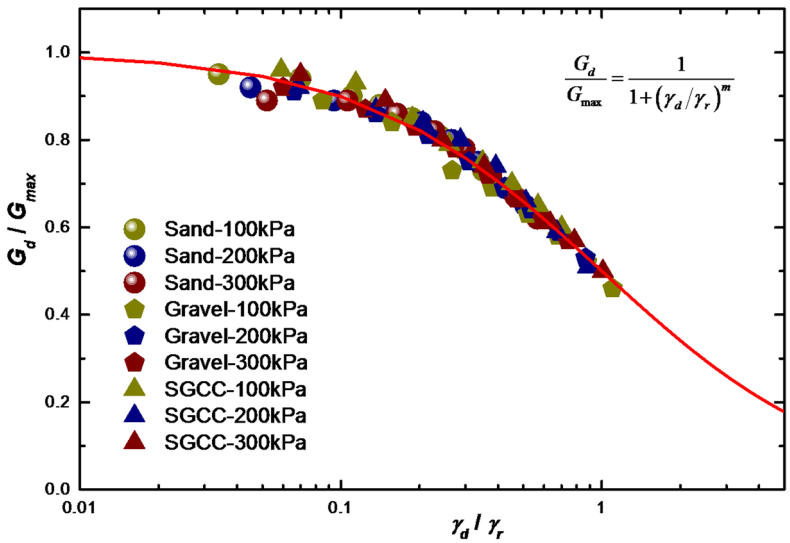

Fig. 12. G_d/G_{max} versus γ_d/γ_r for all samples under different confining pressures.

$$\frac{G_d}{G\max} = \frac{1}{1+(\gamma_d/\gamma_r)^m} \tag{12}$$

where γ_r is the reference dynamic shear strain (i.e. the strain corresponding to G_d/G_{max} =0.5); m is a curve-fitting parameter, determined to be 0.95.

According to the results, the equation effectively captures the dynamic behavior of sand, gravel, and SGCC. The coefficient of determination is R^2 = 0.98, the root mean squared error (Re) is 0.03.

Damping ratio analysis

Figure 13shows the damping ratio results for sand, gravel, and SGCC. Most of the data fall within the range identified by Rollins et al[44]., and they also tend to be located near the lower envelope identified by Seed et al[45].. The variation of the damping ratio with the dynamic shear strain for SGCC is similar to that of sand and gravel. The damping ratio increases with increasing dynamic shear strain and decreases with increasing confining pressure. The reduced damping ratio of SGCC signifies lower energy dissipation per cycle, mainly

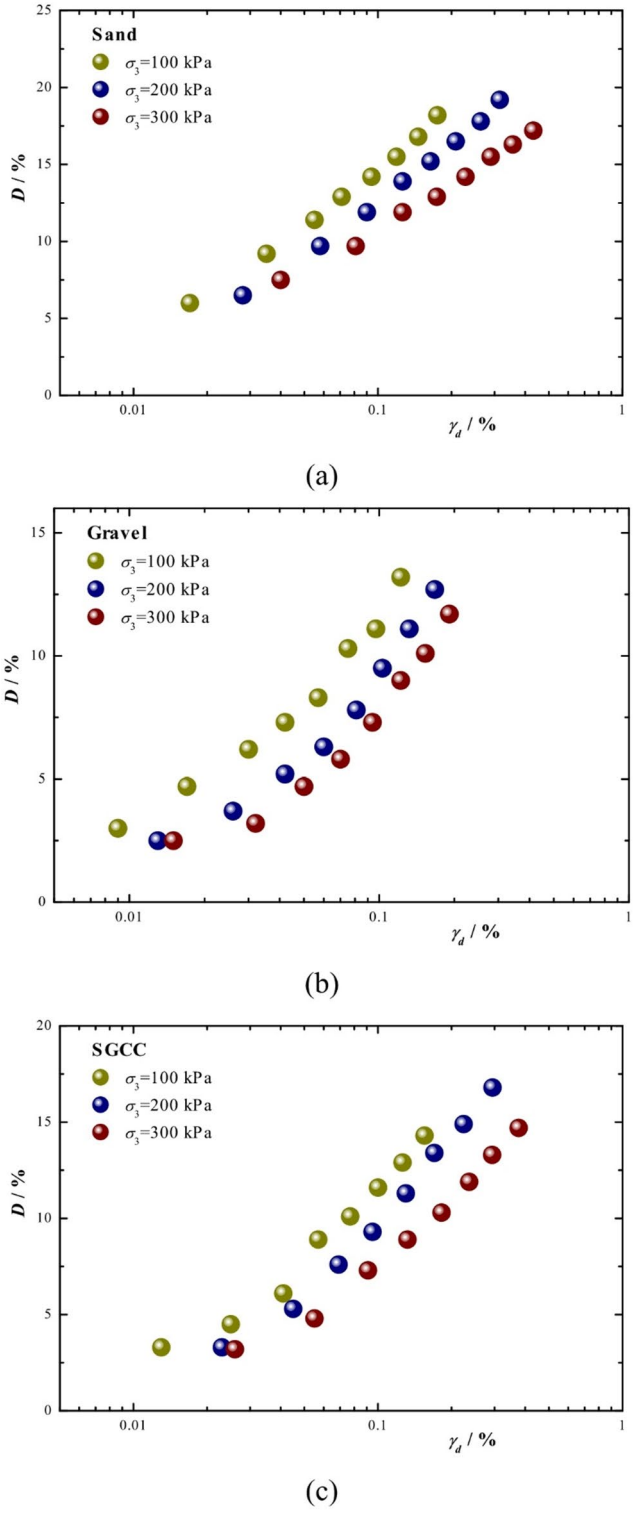

Fig. 13. D versus γ_d relationships for all samples under different confining pressures. (**a**) Sand, (**b**) Gravel, (**c**) SGCC, (**d**) damping ratio to dynamic shear strain.

caused by diminished frictional sliding among sand particles. Rather than dissipating energy via irreversible particle rearrangement—a dominant mechanism in pure sand—more energy is elastically stored within the rigid gravel skeleton and robust sand–gravel interfaces. Consequently, SGCC demonstrates a more elastic and less dissipative behavior under cyclic loading.

The damping ratio is related to dynamic shear strain[46]. Determining the maximum damping ratio is necessary; however, it is difficult to be obtained during testing. Zhu et al[47]. proposed a formula to describe the damping behavior using the damping ratio $D_{0.5}$. Based on their research, a new equation is proposed as follows:

$$D/D_{0.5} = k_d(\gamma_d/\gamma_r)^{n_d} \tag{13}$$

where $D_{0.5}$ is the damping ratio corresponding to G_d/G_{max}=0.5; k_d and n_d are curve-fitting parameters.

The variation of $D/D_{0.5}$ versus γ_d/γ_r is plotted in Fig. 14, with the fitting curves defined by Eq. (13). The coefficients of determination (R^2) for the fitting curves are mostly greater than 0.95, indicating a good agreement with the test data. The fitting parameter k_d for sand, gravel, and SGCC is 1.04, 1.05 and 1.04, respectively, showing minimal differences. However, the differences in the parameter n_d are more pronounced. The n_d values for sand, gravel, and SGCC are 0.38, 0.58 and 0.60, respectively. The values for SGCC are very close to those of gravel.

According to the CMM, the parameters n_d and k_d of SGCC are approximately 1.5 and 1.0 times those of the CMM predictions, respectively, as calculated by the following equations:

$$n_{deq} = n_{dg}A_{rr} + n_{ds}(1 - A_{rr}) \tag{14}$$

$$k_{deq} = k_{dg}A_{rr} + k_{ds}(1 - A_{rr}) \tag{15}$$

where n_{dg} and n_{ds} are the curve-fitting parameters for gravel and sand, respectively; k_{dg} and k_{ds} are the corresponding curve-fitting parameters for gravel and sand.

Dynamic strength analysis

The dynamic strength of soil refers to the magnitude of dynamic shear stress required to cause soil failure under a given number of vibration cycles. Figure 15 shows the relationship between dynamic shear stress and the number of failure cycles (N_f) for sand, gravel, and SGCC.

The dynamic strength of gravel is the highest, followed by SGCC, while sand exhibits the lowest strength. The results indicate that incorporating gravel columns into the sand can enhance its dynamic strength. The relationship between dynamic shear stress ratio (τ_d/σ_3') and the number of failure cycles is approximately linear, as expressed by:

$$\tau_d/\sigma_3' = k_1 - k_2 \ln(N_f) \tag{16}$$

where k_1 and k_2 are curve-fitting parameters.

According to the results, the proposed equation can better reflect the influence of the number of failure cycles on the dynamic shear stress ratio. The fitting parameters k_1 and k_2 for SGCC are 0.484 and 0.064, respectively, which are approximately 1.1 times those of the sand. The correlation coefficient (R^2) is 0.98, as shown in Fig. 15(b).

Figure 16 shows the relationship between dynamic axial strain and the number of loading cycles for sand, gravel, and SGCC under cyclic loading. During the initial few vibration cycles, the samples primarily undergo elastic deformation with minimal plastic deformation, and the amplitude of dynamic axial strain amplitude

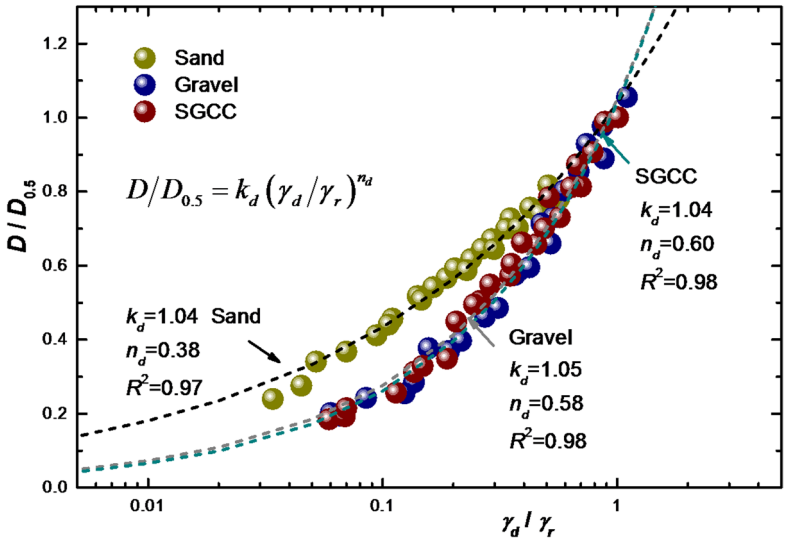

Fig. 14. $D/D_{0.5}$ versus γ_d/γ_r for all samples under different confining pressures.

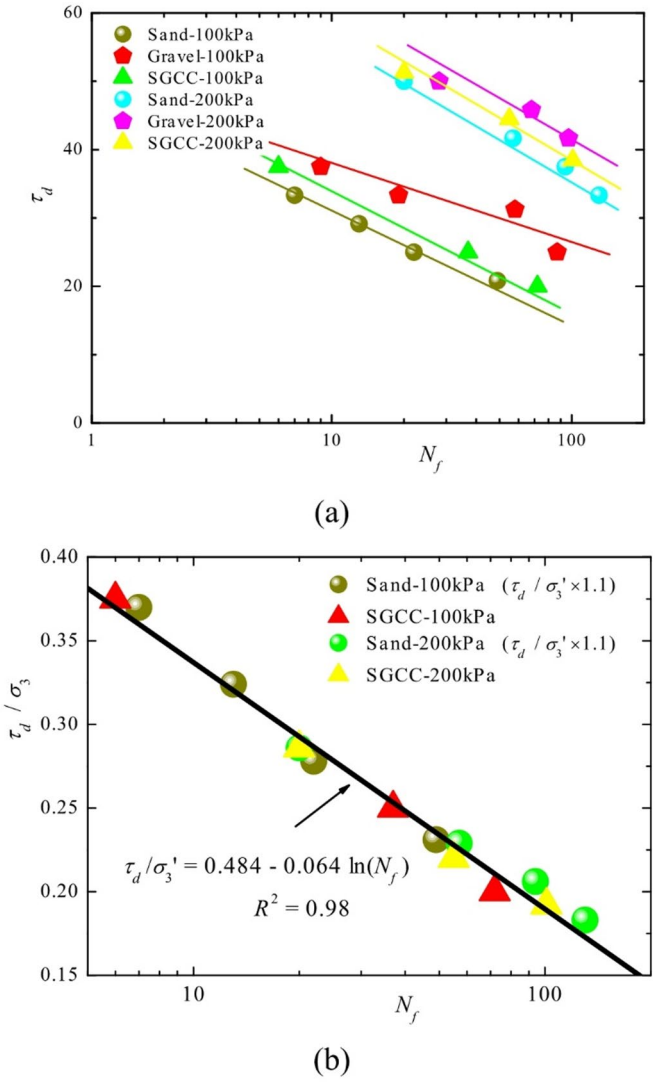

Fig. 15. Dynamic shear stress ratio versus Number of cycles of failure. (**a**) τd vs. Nf, (**b**) τd/σ3 vs. Nf.

remains low. With an increasing number of cycles, the strain develops steadily. For SGCC, the dynamic axial strain beings to increase sharply when the number of cycles reaches approximately 30, indicating the onset of instability. When the number of cycles reaches 53, the maximum dynamic axial strain exceeds 5%, and the specimen reaches the failure state.

The test results indicate that the addition of gravel to the sand sample improves its resistance to deformation. The number of vibration cycles at the onset of instability is 9 for sand and 21 for gravel.

The development of pore water pressure (σ_u) under vibrational loading is an important factor affecting soil deformation and strength. An increase in pore water pressure leads to a reduction in shear strength, which can ultimately result in large deformations and soil failure. The relationships between normalized pore water pressure and normalized number of failure cycles (N/N_f) for sand, gravel, and SGCC at $\sigma_3 = 100$ kPa are shown in Fig. 17. The figure reveals distinct patterns of pore pressure generation for sand, gravel, and SGCC on their path to failure. For the tests presented, the behavior of SGCC is similar to that of sand. With increasing N/N_f, the pore water pressure initially increases slowly (N/N_f=0~0.15), then grows rapidly (N/N_f=0.15 ~ 0.8), and finally increases slowly again (N/N_f=0.8 ~ 1.0). Compared to sand, the pore water pressure development in SGCC can be divided into two segments during the rapid growth phase. When N/N_f ranges from 0.15 to 0.55, the growth pattern of SGCC is similar to that of gravel.

The primary role of the SGCC is to enhance liquefaction resistance through improved drainage, increased shear strength, and greater dilation capacity. This composite reinforcement significantly delays failure, enabling the soil to withstand more loading cycles before reaching failure. The behavior of SGCC is consistent with previous findings for sand-gravel mixtures[48].

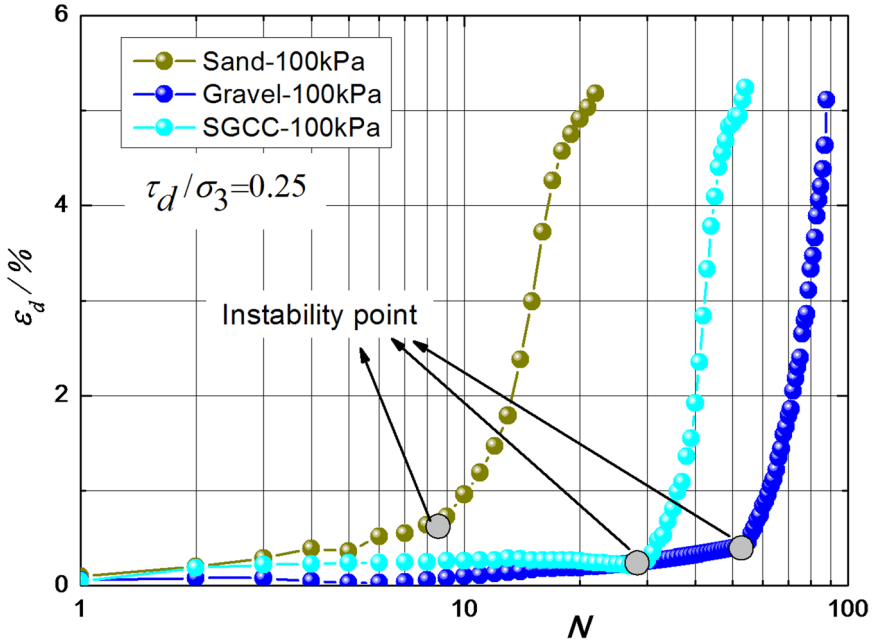

Fig. 16. Dynamic shear strain versus Number of cycles of failure.

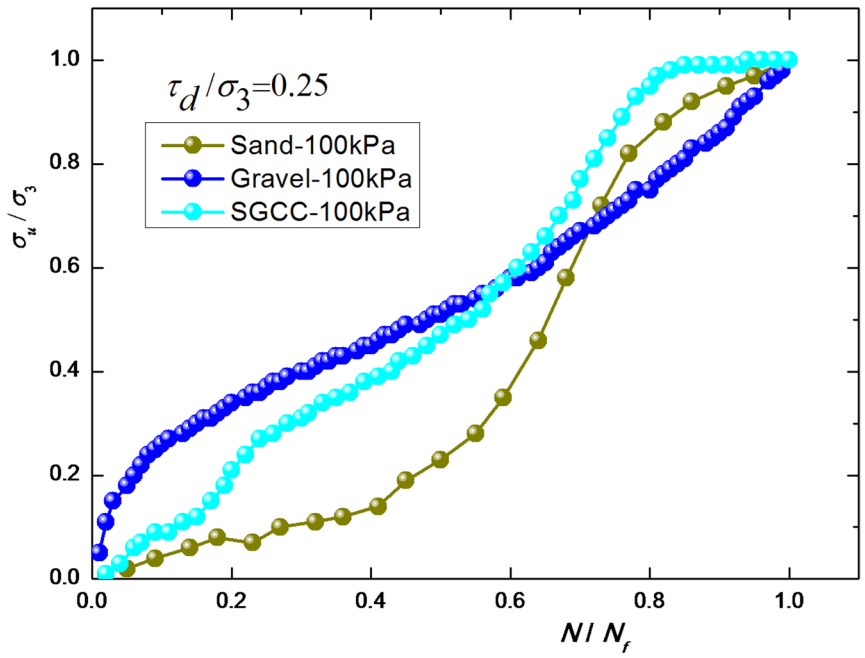

Fig. 17. Normalized pore water pressure versus normalized number of failure cycles.

Engineering implications and future work

It should be noted that this study primarily focuses on element-scale experimental investigation aimed at elucidating the strength and deformation mechanisms of SGCC. While the experimental results cannot be directly extrapolated to prototype-scale applications without further validation through large-scale model tests or field monitoring, the mechanistic understanding established in this research provides significant value for engineering practice. The revealed relationships, particularly the dependence of the strength improvement ratio on confining pressure and the proposed correction factors for the CMM, offer a solid theoretical basis for enhancing the design methodology and analytical framework for stone column-reinforced composite foundations.

While this study offers fundamental insights derived from laboratory tests, its findings provide valuable guidance for enhancing stone column design methodologies. The empirical relationships and correction factors established here, particularly the confining pressure-dependent strength ratio and refined CMM parameters, provide a theoretical foundation for improving predictive models. It should be noted that direct application to field-scale designs requires further validation through large-scale model tests and field monitoring, which constitute the next phase of this research. Nevertheless, the mechanistic understanding obtained from this experimental study offers important insights for optimizing stone column design and improving numerical simulations of composite foundation behavior.

A limitation of this study is that the experimental results were primarily evaluated against the CMM. While this approach offers valuable validation of the CMM's predictive performance, future work should compare these findings with other advanced predictive models and detailed numerical simulations to enhance the generalizability of the conclusions and support the development of more robust design guidelines. Such comparative analyses would help establish the broader applicability of the proposed correction factors and yield further insight into the complex interactions within composite foundations.

Conclusions

(1) The incorporation of gravel columns enhances the strength of sand samples. Under drained conditions, the strength improvement of SGCC shows a negative correlation with confining pressure, whereas under undrained conditions, the strength increase exhibits a positive correlation with confining pressure.

(2) In CD test, the inclusion of gravel in the sand samples suppresses dilatancy at large strains and reduces sample deformation. However, this effect diminishes with increasing confining pressure. In CU test, SGCC exhibits higher excess pore pressure than sand at small strains, but as the strain increases, the pore pressure of both materials tends to converge. The failure stress ratio of SGCC lies between those of sand and gravel, and exceeds the value predicted by CMM.

(3) The dynamic shear modulus and damping ratio characteristics of SGCC follow trends similar to those of sand and gravel, and conform to a normalized hyperbolic model. The inclusion of gravel columns increases the dynamic shear modulus and reduces the damping ratio. The modulus coefficient k and damping parameter n_d for SGCC are 1.2 and 1.5 times, respectively, those predicted by CMM.

(4) Gravel columns do not significantly mitigate pore water pressure accumulation. The dynamic strength of SGCC is 1.1 times that of sand. The development of pore water pressure in SGCC with normalized cycle number (N/N_f) can be divided into four distinct stages.

(5) This study provides practical insights for stone column design: the proposed CMM correction factors enable more accurate design calculations; the established confining pressure-efficiency relationship guides depth-dependent optimization; and the characterized dynamic properties enhance seismic safety evaluations.

Data availability

"All data generated or analysed during this study are included in this published article."

Received: 25 July 2025; Accepted: 24 October 2025
Published online: 25 November 2025

References

1. Hughes, J. M. O., Withers, N. J. & Greenwood, D. A. A. Field trial of the reinforcing effect of a stone column in soil. *Geotechnique* **25**, 31–44 (1975).
2. Ng, K. S. & Tan, S. A. Simplified homogenization method in stone column designs. *Soils Found.* **55**, 154–165 (2015).
3. Almeida, M. et al. Stone columns field test: monitoring data and numerical analyses. *Geotech. Eng.* **45**, 103–112 (2014).
4. Zou, T. N., Wang, J., Dong, L. & Chen, F. C. Application of digital monitoring system of stone column piles in airport construction. IOP Conference Series: Earth and Environmental Science 643, (2021).
5. Ghazavi, M. & Afshar, J. N. Bearing capacity of geosynthetic encased stone columns. *Geotext. Geomembr.* **38**, 26–36 (2013).
6. Murugesan, S. & Rajagopal, K. Performance of encased stone columns and design guidelines for construction on soft clay soils. Geosynthetics in Civil and Environmental Engineering - Geosynthetics Asia 2008: Proceedings of the 4th Asian Regional Conference on Geosynthetics 729–734 (2008).
7. El-Garhy, B., Maraie, M. & Youssef, A. F. Behavior of model footings resting on soft clay reinforced by floating granular piles: experimental study. *Int. J. Geotech. Eng.* **5**, 415–424 (2011).
8. Black, J., Sivakumar, V. & McKinley, J. D. Performance of clay samples reinforced with vertical granular columns. *Can. Geotech. J.* **44**, 89–95 (2007).
9. Chenari, R. J., Fard, M. K., Chenari, M. J. & Sosahab, J. S. Physical and numerical modeling of stone column behavior in loose sand. *Int. J. Civil Eng.* **17**, 231–244 (2019).
10. Xu, F., Moayedi, H., Foong, L. K., Moghadam, M. J. & Zangeneh, M. Laboratory and numerical analysis of geogrid encased stone columns. *Measurement* **169**, 108369 (2021).
11. Alfaro, M. C., Blatz, J. A., Abdulrazaq, W. F. & Kim, C. Evaluating shear mobilization in rockfill columns used for riverbank stabilization. *Can. Geotech. J.* **46**, 976–986 (2009).
12. Adalier, K. & Elgamal, A. Mitigation of liquefaction and associated ground deformations by stone columns. *Eng. Geol.* **72**, 275–291 (2004).
13. Black, J. A., Sivakumar, V. & Bell, A. The settlement performance of stone column foundations. *Geotechnique* **61**, 909–922 (2011).
14. Ambily, A. P. & Gandhi, S. R. Behavior of stone columns based on experimental and FEM analysis. *J. Geotech. GeoEnviron. Eng.* **133**, 405–415 (2007).
15. Singh, I. & Sahu, A. K. Multi-blended granular columns encased with geosynthetics. *Z. Der Deutschen Gesellschaft Fur Geowissenschaften*. **175**, 73–88 (2024).
16. Yang, F. O. et al. A large-scale shaking table model test for acceleration and deformation response of geosynthetic encased stone column composite ground. *Geotext. Geomembr.* **49**, 1407–1418 (2021).
17. Ashour, S., Ghataora, G. & Jefferson, I. Behaviour of model stone column subjected to Cyclic loading. *Transp. Geotechnics*. **35**, 100777 (2022).

18. Sasaki, Y. & Taniguchi, E. Shaking table tests on gravel drains to prevent liquefaction of sand deposits. *Japanese Soc. Soil. Mech. Foundation Eng.* **22**, 1–14 (1982).
19. Huang, C. X., Sui, Z. L., Wang, L. & Liu, K. F. Mitigation of soil liquefaction using stone columns: an experimental investigation. *Mar. Georesour. Geotechnol.* **34**, 244–251 (2016).
20. Badanagki, M., Dashti, S. & Kirkwood, P. Influence of dense granular columns on the performance of level and gently sloping liquefiable sites. *J. Geotech. GeoEnviron. Eng.* **144**, 04018065 (2018).
21. Dashti, S., Bray, J. D., Pestana, J. M., Riemer, M. & Wilson, D. Centrifuge testing to evaluate and mitigate liquefaction-induced Building settlement mechanisms. *J. Geotech. GeoEnviron. Eng.* **136**, 918–929 (2010).
22. Gu, Z. A., Niu, F. J., Chen, J. F. & Wang, X. T. Centrifuge tests on geosythetic-encased stone column supported embankement on seasonal frozen soil. *Geotext. Geomembr.* **50**, 922–931 (2022).
23. Li, P., Dashti, S., Badanagki, M. & Kirkwood, P. Evaluating 2D numerical simulations of granular columns in level and gently sloping liquefiable sites using centrifuge experiments. *Soil Dyn. Earthq. Eng.* **110**, 232–243 (2018).
24. Chen, L. H., Zhang, T. M., Lin, T. H., Zhou, X. G. & Chen, Z. Y. Consolidation and stability behaviour of a high rockfill dam built on soft clay foundation. Proceeding of 3rd International Conference on soft soil engineering ICSSE3 175–180 (2001).
25. Liu, S. H., Wang, L. J., Wang, Z. J. & Bauer, E. Numerical stress-deformation analysis of cut-off wall in clay-core rockfill dam on Thick overburden. *Water Sci. Eng.* **9**, 219–226 (2016).
26. Mashiri, M. S., Vinod, J. S. & Sheikh, M. N. Liquefaction potential and dynamic properties of sand-tire chip (STCh) mixture. *Geotech. Test. J.* **39**, 69–79 (2016).
27. Chen, J. F., Wang, X. T., Xue, J. F., Zeng, Y. & Feng, S. Z. Uniaxial compression behavior of geotextile encased stone columns. *Geotext. Geomembr.* **46**, 277–283 (2018).
28. Pandey, B. K., Rajesh, S. & Chandra, S. Electrokinetics in a stone column encased by a conductive jute geotextile: the role of anode materials. *Int. J. Geomech.* **24**, 04024095 (2024).
29. Fan, G. L., Nasiri, M. & Amiri, E. Stabilized slope using stone columns reinforced with geotextile encasement and laminated coatings: a case study. *Nat. Hazards Rev.* **26**, 1–13 (2025).
30. Pavan, B. & Rathod, D. Experimental and numerical studies on 3D cellular confinements supported over an encased group of stone columns. *Int. J. Geomech.* **25**, 04025102 (2025).
31. Najjar, S. S., Sadek, S. & Maakaroun, T. Effect of sand columns on the undrained load response of soft clays. *J. Geotech. GeoEnviron. Eng.* **136**, 1263–1277 (2010).
32. Cai, X. C., Zhang, L., Yang, Z. J. & Mao, B. B. Dynamic behavior of GESC groups in sand under sinusoidal loading: a continuum-discrete coupled analysis. *Int. J. Numer. Anal. Meth. Geomech.* 2655–2669 (2025).
33. Gu, M. X., Cai, X. C., Qiu, J. C., Zhang, X. Y. & Han, D. L. Dynamic behavior of stone column–improved soft clay under three-stage traffic loads. *Int. J. Geomech.* **25**, 04024322 (2025).
34. MWR GB/T 50123 – 2019. *Standard for Geotechnical Testing Method* (China Planning, 2019).
35. Asgari, A., Oliaei, M. & Bagheri, M. Numerical simulation of improvement of a liquefiable soil layer using stone column and pile-pinning techniques. *Soil Dyn. Earthq. Eng.* **51**, 77–96 (2013).
36. Abusharar, S. W. & Han, J. Two-dimensional deep-seated slope stability analysis of embankments over stone column-improved soft clay. *Eng. Geol.* **120**, 103–110 (2011).
37. Zhang, Z., Han, J. & Ye, G. B. Numerical investigation on factors for deep-seated slope stability of stone column-supported embankments over soft clay. *Eng. Geol.* **168**, 104–113 (2014).
38. Akbarimehr, D. & Fakharian, K. Dynamic shear modulus and damping ratio of clay mixed with waste rubber using Cyclic triaxial apparatus. *Soil Dyn. Earthq. Eng.* **140**, 106435 (2021).
39. Yang, G., Liu, K. L. & Liu, H. L. Dynamic deformation behaviour of coarse aggregate under Cyclic loading by PFC3D. *Eur. J. Environ. Civil Eng.* **17**, 282–293 (2013).
40. Chen, G. X., Pan, H., Long, H. & Li, X. J. Dynamic constitutive model for soils considering asymmetry of skeleton curve. *J. Rock Mech. Geotech. Eng.* **5**, 400–405 (2013).
41. Meidani, M. et al. Granule shear effect on the shear modulus and damping ratio of mixed gravel and clay. *Iran. J. Sci. Technol.* **32**, 501–518 (2008).
42. Zhou, W., Chen, Y., Ma, G., Yang, L. F. & Chang, X. L. A modified dynamic shear modulus model for rockfill materials under a wide range of shear strain amplitudes. *Soil Dyn. Earthq. Eng.* **92**, 229–238 (2017).
43. Stokoe, K. H., Darendeli, M. B., Andrus, R. D. & Brown, L. T. Dynamic soil properties: laboratory, field and correlation studies. International Conference on earthquake geotechnical engineering 6, 811–845 (1999).
44. Rollins, K. M., Evans, M. D. & Diehl, N. B. Daily III, W. D. Shear modulus and damping relationships for gravels. *J. Geotech. GeoEnviron. Eng.* **124**, 396–405 (1998).
45. Seed, B. H. B., Wong, R. T., Idriss, I. M. & Tokimatsu, K. Moduli and damping factors for dynamic analyses of cohesionless soils. *J. Geotech. Eng.* **112**, 1016–1032 (1986).
46. Hardin, B. O. & Drnevich, V. P. Shear modulus and damping in soils: measurement and parameter effects. *J. Soil. Mech. Found. Div.* **98**, 603–624 (1972).
47. Zhu, S., Yang, G., Wen, Y. & Ou, L. Dynamic shear modulus reduction and damping under high confining pressures for gravels. *Geotechnique Lett.* **4**, 179–186 (2014).
48. Amini, F. & Chakravrty, A. Liquefaction testing of layered Sand-Gravel composites. *Geotech. Test. J.* **27**, 1–11 (2009).

Acknowledgements

The financial support provided by the National Natural Science Foundation of China (No. 51479059) is greatly appreciated.

Author contributions

Author ContributionsG.Y. and Q.F. conceived the research and designed experiments; J.G. performed analysis of static triaxial test results; Y.Z. performed analysis of dynamic triaxial test results; G.Y. wrote the original draft and supervised the research; All authors reviewed and approved the final manuscript. Correspondence to: G.Y.

Declarations

Competing interests

The authors declare no competing interests.

Additional information

Correspondence and requests for materials should be addressed to G.Y.

Reprints and permissions information is available at www.nature.com/reprints.

Publisher's note Springer Nature remains neutral with regard to jurisdictional claims in published maps and institutional affiliations.

Open Access This article is licensed under a Creative Commons Attribution-NonCommercial-NoDerivatives 4.0 International License, which permits any non-commercial use, sharing, distribution and reproduction in any medium or format, as long as you give appropriate credit to the original author(s) and the source, provide a link to the Creative Commons licence, and indicate if you modified the licensed material. You do not have permission under this licence to share adapted material derived from this article or parts of it. The images or other third party material in this article are included in the article's Creative Commons licence, unless indicated otherwise in a credit line to the material. If material is not included in the article's Creative Commons licence and your intended use is not permitted by statutory regulation or exceeds the permitted use, you will need to obtain permission directly from the copyright holder. To view a copy of this licence, visit http://creativecommons.org/licenses/by-nc-nd/4.0/.

© The Author(s) 2025